Chapter 6

Comprehensive Analytical Models of Random Variations in Subthreshold MOSFET's High-Frequency Performances

Rawid Banchuin

Additional information is available at the end of the chapter

http://dx.doi.org/10.5772/intechopen.72710

Abstract

Subthreshold MOSFET has been adopted in many low power VHF circuits/systems in which their performances are mainly determined by three major high-frequency characteristics of intrinsic subthreshold MOSFET, i.e., gate capacitance, transition frequency, and maximum frequency of oscillation. Unfortunately, the physical level imperfections and variations in manufacturing process of MOSFET cause random variations in MOSFET's electrical characteristics including the aforesaid high-frequency ones which in turn cause the undesired variations in those subthreshold MOSFET-based VHF circuits/systems. As a result, the statistical/variability aware analysis and designing strategies must be adopted for handling these variations where the comprehensive analytical models of variations in those major high-frequency characteristics of subthreshold MOSFET have been found to be beneficial. Therefore, these comprehensive analytical models have been reviewed in this chapter where interesting related issues have also been discussed. Moreover, an improved model of variation in maximum frequency of oscillation has also been proposed.

Keywords: gate capacitance, maximum frequency of oscillation, subthreshold MOSFET, transition frequency, VHF circuits/systems

1. Introduction

Subthreshold MOSFET has been extensively used in many VHF circuits/systems, e.g., wireless microsystems [1], low power receiver [2], low power LNA [3, 4] and RF front-end [5], where performances of these VHF circuits/systems are mainly determined by three major high-frequency characteristics of intrinsic subthreshold MOSFET, i.e., gate capacitance, C_g, transition frequency, f_T, and maximum frequency of oscillation, f_{max}. Clearly, the physical level imperfections and manufacturing process variations of MOSFET, e.g., gate length random

fluctuation, line edge roughness, random dopant fluctuation, etc., cause the variations in MOSFET's electrical characteristics, e.g., drain current, I_D and transconductance, g_m, etc. These variations are crucial in the statistical/variability aware analysis and design of MOSFET-based circuits/systems. So, there exist many previous studies on such variations which some of them have also focused on the subthreshold MOSFET [1, 6–12]. Unfortunately, C_g, f_T, and f_{max} have not been considered even though they also exist and greatly affect the high-frequency performances of such MOSFET-based circuits/systems. Therefore, analytical models of variations in those major high-frequency characteristics have been performed [13–17]. In [13], an analytical model of variation in f_T derived as a function of the variation in C_g has been proposed where only strong inversion MOSFET has been focused. However, this model is not comprehensive, as none of any related physical levels variable of the MOSFET has been involved. In [14], the models of variations in C_g and f_T, which are comprehensive as they are in terms of the related MOSFET's physical level variables, have been proposed. Again, only the strong inversion MOSFET has been considered in [14].

According to the aforementioned importance and usage of subthreshold MOSFET in the MOSFET-based VHF circuits/systems, the comprehensive analytical models of variations in C_g, f_T, and f_{max} of subthreshold MOSFET have been proposed [15–17]. Such models have been found to be very accurate as they yield smaller than 10% the average percentages of errors. In this chapter, the revision of these models will be made where some foundations on the subthreshold MOSFET will be briefly given in the subsequent section followed by the revision on models of C_g in Section 3. The models of f_T and f_{max} will, respectively, be reviewed in Sections 4 and 5 where an improved model of variation in f_{max} will also be introduced. Some interesting issues related to these models will be mentioned in Section 6 and the conclusion will be finally drawn in Section 7.

2. Foundations on subthreshold MOSFET

Unlike the strong inversion MOSFET in which I_d is a polynomial function of the gate to source voltage, V_{gs}, I_d of the subthreshold MOSFET is an exponential function of V_{gs} and can be given as follows:

$$I_d = \mu C_{dep} \frac{W}{L} \left(\frac{kT}{q}\right)^2 \exp\left[\frac{V_{gs} - V_t}{nkT/q}\right] \left[1 - \exp\left[-\frac{V_{ds}}{kT/q}\right]\right] \tag{1}$$

where C_{dep} and n denote the capacitance of the depletion region under the gate area and the subthreshold parameter, respectively.

By using Eq. (1) and keeping in mind that $g_m = dI_d/dV_{gs}$, g_m of subthreshold MOSFET can be given by

$$g_m = \frac{\mu}{n} C_{dep} \frac{W}{L} \left(\frac{kT}{q}\right)^2 \exp\left[\frac{V_{gs} - V_t}{nkT/q}\right] \left[1 - \exp\left[-\frac{V_{ds}}{kT/q}\right]\right] \tag{2}$$

http://dx.doi.org/10.5772/intechopen.72710

3. Variation in gate capacitance (C_g)

Before reviewing the models of variation in C_g of subthreshold MOSFET, it is worthy to introduce the mathematical expression of C_g as it is the mathematical basis of such models. Here, C_g which can be defined as the total capacitance seen by looking in to the gate terminal of the MOSFET as shown in **Figure 1**, can be given in terms of the gate charge, Q_g as [15]

$$C_g = \frac{dQ_g}{dV_{gs}} \tag{3}$$

where

$$Q_g = \frac{\mu W^2 L C_{ox}^2}{I_d} \int_0^{Vgs-Vt} \left(V_{gs} - V_c - V_t\right)^2 dV_c - Q_{B,max} \tag{4}$$

It is noted that $Q_{B,max}$ stands for the maximum bulk charge [15]. By using Eq. (1), Q_g of the subthreshold MOSFET can be found as

$$Q_g = \frac{\left[\frac{WL^2 C_{ox}^2}{C_{dep}(kT/q)^2}\right]\left(V_{gs} - V_t\right)^3}{3\left[1 - \exp\left[-\frac{V_{ds}}{kT/q}\right]\right]\exp\left[\frac{q}{nkT}\left(V_{gs} - V_t\right)\right]} - Q_{B,max} \tag{5}$$

As a result, the expression of C_g can be obtained by using Eqs. (1) and (5) as follows

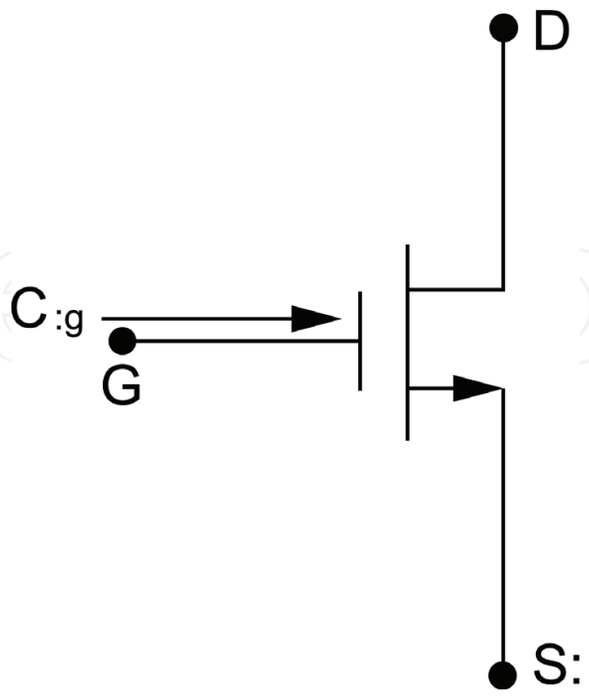

Figure 1. The conceptual definition of C_g (referenced to N-type MOSFET).

$$C_g = \frac{1}{3}\left[\frac{WL^2C_{ox}^2}{C_{dep}(kT/q)^2}\right]\left[3(V_{gs}-V_t)^2 - \frac{q}{nkT}(V_{gs}-V_t)^3\right]\exp\left[-\frac{q}{nkT}(V_{gs}-V_t)\right] \tag{6}$$

By taking the physical level imperfections and manufacturing process variations of MOSFET into account, random variations in MOSFET's parameters such as V_t, W, L, etc., denoted by ΔV_t, ΔW, ΔL, and so on existed. These variations yield the randomly varied C_g i.e. $C_g(\Delta V_t, \Delta W, \Delta L, \ldots)$ [15]. Thus, the variations in C_g, ΔC_g can be mathematically defined as [15]

$$\Delta C_g \triangleq C_g(\Delta V_t, \Delta W, \Delta L, \ldots) - C_g \tag{7}$$

where C_g stands for the nominal gate capacitance in this context.

With this mathematical definition and the fact that ΔV_t is the most influential in subthreshold MOSFET [18], the following comprehensive analytical expression of ΔC_g has been proposed in [15]

$$\Delta C_g = 2\left[\sqrt{\frac{W}{C_{dep}}}\frac{LC_{ox}}{kT/q}\right]^2\left[\exp\left[-\frac{V_{ds}}{kT/q}\right]-1\right]^{-1} \left[V_{gs}-V_{FB}-\phi_s-N_{eff}W_{dep}\right]\left[V_t-V_{FB}-\phi_s-N_{eff}W_{dep}\right] \tag{8}$$

where N_{eff}, V_{FB}, W_{dep}, and ϕ_s denote the effective values of the substrate doping concentration $N_{sub}(x)$, the flat band voltage, depletion width, and surface potential, respectively. Moreover, N_{eff} can be obtained by weight averaging of $N_{sub}(x)$ as [15]

$$N_{eff} = 3\int_0^{W_{dep}} N_{sub}(x)\left(1-\frac{x}{W_{dep}}\right)^2\frac{dx}{W_{dep}} \tag{9}$$

As ΔC_g is a random variable, it is necessary to derive its statistical parameters for completing the comprehensive analytical modeling. Among various statistical parameters, the variance has been chosen as it determines the spread of the variation in a convenient manner. Based on the traditional analytical model of statistical variation in MOSFET's parameter [19], the variances of ΔC_g, $Var[\Delta C_g]$ can be analytically obtained as follows [15]

$$Var[\Delta C_g] = \frac{8q4N_{eff}W_{dep}WL}{\varepsilon_0^2k^2T^2C_{dep}^2}\left[\exp\left[-\frac{V_{ds}}{kT/q}\right]-1\right]^{-2}\left[V_{gs}-V_{FB}-\phi_s-N_{eff}W_{dep}\right]^2 \tag{10}$$

where ε_0 stands for the permittivity of free space. At this point, it can be seen that the comprehensive analytical model of ΔC_g proposed in [15] is composed of Eqs. (8) and (10) where the latter has been derived based on the former. In [15], $(Var[\Delta C_g])^{0.5}$ calculated by using the proposed model has been compared to its 65 nm CMOS technology-based benchmarks obtained by using the Monte Carlo simulation for verification where strong agreements between the model-based $(Var[\Delta C_g])^{0.5}$ and the benchmark have been found. The average

deviation from the benchmark obtained from the entire range of V_{gs} used for simulation given by 0–100 mV has been found to be 9.42565 and 8.91039% for N-type and P-type MOSFET-based comparisons, respectively [15].

Later, an improved model of ΔC_g has been proposed in [16] where the physical level differences between N-type and P-type MOSFETs, e.g., carrier type, etc., has also been taken into account. Such model is composed of the following equations

$$\Delta C_{gN} = 2\left[\sqrt{\frac{W}{C_{dep}}}\frac{LC_{ox}}{kT/q}\right]^2\left[\exp\left[-\frac{V_{ds}}{kT/q}\right]-1\right]^{-1}\left[V_{gs}-V_{FB}-2\phi_F-C_{ox}^{-1}\sqrt{2q\varepsilon_{Si}N_a\left(2\phi_F+V_{sb}\right)}\right] \times \left[V_t-V_{FB}-2\phi_F-C_{ox}^{-1}\sqrt{2q\varepsilon_{Si}N_a\left(2\phi_F+V_{sb}\right)}\right] \tag{11}$$

$$\Delta C_{gP} = 2\left[\sqrt{\frac{W}{C_{dep}}}\frac{LC_{ox}}{kT/q}\right]^2\left[\exp\left[-\frac{V_{ds}}{kT/q}\right]-1\right]^{-1}\left[V_{gs}-V_{FB}+\left|2\phi_F\right|+C_{ox}^{-1}\sqrt{2q\varepsilon_{Si}N_d\left(\left|2\phi_F\right|-V_{sb}\right)}\right] \times \left[V_t-V_{FB}+\left|2\phi_F\right|+C_{ox}^{-1}\sqrt{2q\varepsilon_{Si}N_d\left(\left|2\phi_F\right|-V_{sb}\right)}\right)] \tag{12}$$

$$Var\left[\Delta C_{gN}\right] = \frac{12q^6N_{eff}W_{dep}WL^3}{C_{dep}^2}\left(\frac{C_{ox}}{kT}\right)^4\left[1-\exp\left[-\frac{V_{ds}}{kT/q}\right]\right]^{-2} \frac{\left[V_{gs}-V_{FB}-2\phi_F-C_{ox}^{-1}\sqrt{2q\varepsilon_{Si}N_a\left(2\phi_F+V_{sb}\right)}\right]^2}{V_t^{-1}\left[V_{FB}+2\phi_F+C_{ox}^{-1}\sqrt{2q\varepsilon_{Si}N_a\left(2\phi_F+V_{sb}\right)}\right]} \tag{13}$$

$$Var\left[\Delta C_{gP}\right] = \frac{12q^6N_{eff}W_{dep}WL^3}{C_{dep}^2}\left(\frac{C_{ox}}{kT}\right)^4\left[1-\exp\left[-\frac{V_{ds}}{kT/q}\right]\right]^{-2} \frac{\left[V_{gs}-V_{FB}+\left|2\phi_F\right|+C_{ox}^{-1}\sqrt{2q\varepsilon_{Si}N_d\left(\left|2\phi_F\right|-V_{sb}\right)}\right]^2}{V_t^{-1}\left[V_{FB}-\left|2\phi_F\right|-C_{ox}^{-1}\sqrt{2q\varepsilon_{Si}N_d\left(\left|2\phi_F\right|-V_{sb}\right)}\right]} \tag{14}$$

where ΔC_{gN} and ΔC_{gP} are ΔC_g of N-type and P-type MOSFETs, respectively. Moreover, N_a, N_d, V_{sb}, and ϕ_F denote acceptor doping density, donor doping density, source to body voltage, and Fermi potential, respectively [16]. Also, it is noted that Eqs. (13) and (14) have been, respectively, derived by using Eqs. (11) and (12) based on the up-to-date analytical model of statistical variation in MOSFET's parameter [20] instead of the traditional one.

In [16], a verification similar to that of [15] has been made, i.e., $(Var[\Delta C_{gN}])^{0.5}$ and $(Var[\Delta C_{gP}])^{0.5}$ have been, respectively, compared with their 65 nm CMOS technology-based benchmarks. Both $(Var[\Delta C_{gN}])^{0.5}$ and $(Var[\Delta C_{gP}])^{0.5}$ have been calculated by using the proposed model, and the benchmarks have been obtained from the Monte Carlo simulation. The comparison results have been redrawn here in **Figures 2** and **3** where strong agreements with their benchmarks of the model-based $(Var[\Delta C_{gN}])^{0.5}$ and $(Var[\Delta C_{gP}])^{0.5}$ can be seen for the whole range of V_{gs}. The

average deviations determined from such range have been found to be 8.45033 and 6.53211%, respectively [16], which are lower than those of the previous model proposed in [15]. Therefore, the model proposed in [16] has also been found to be more accurate than its predecessor

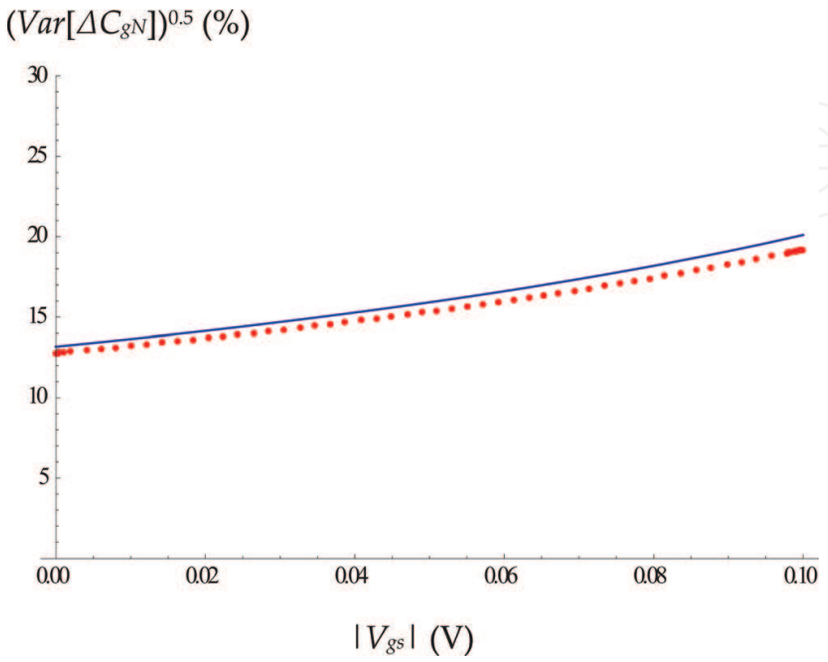

Figure 2. Comparative plot of the model-based $(Var[\Delta C_{gN}])^{0.5}$ (line) and the Monte Carlo simulation-based $(Var[\Delta C_{gN}])^{0.5}$ (dotted) with respect to V_{gs} [16].

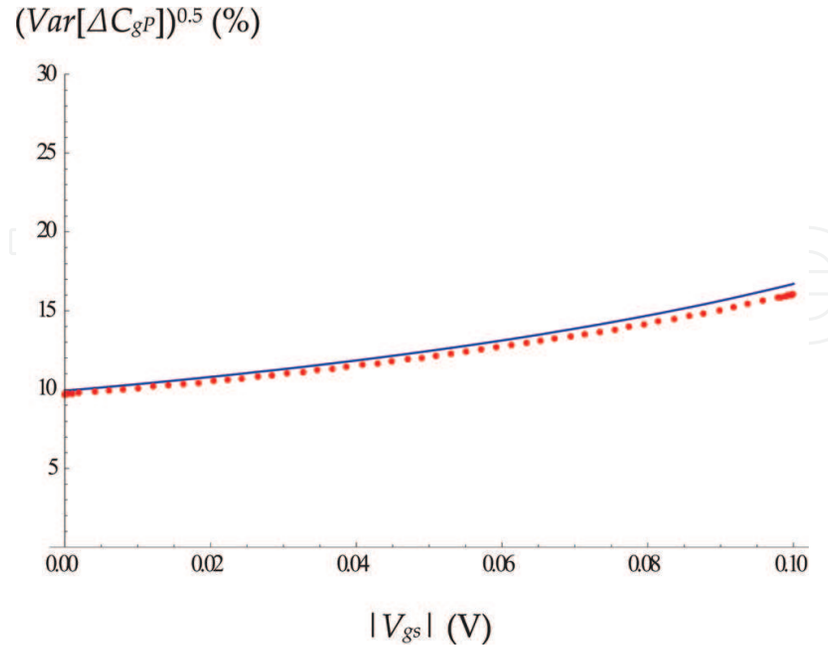

Figure 3. Comparative plot of the model-based $(Var[\Delta C_{gP}])^{0.5}$ (line) and the Monte Carlo simulation-based $(Var[\Delta C_{gP}])^{0.5}$ (dotted) with respect to V_{gs} [16].

[15] apart from being more detailed as the physical level differences between N-type and P-type MOSFETs have also been taken into account.

4. Variation in transition frequency (f_T)

Apart from that of ΔC_g, the comprehensive analytical model of variation in f_T of subthreshold MOSFET, Δf_T has also been proposed in [16]. Before reviewing such model, it is worthy to show the definition of f_T and its comprehensive analytical expression derived in [16]. According to [21], f_T can be defined as the frequency at which the small-signal current gain of the device drops to unity, while the source and drain terminals are held at ground and can be related to C_g by the following equation [13]

$$f_T = \frac{g_m}{2\pi C_g} \tag{15}$$

By using Eqs. (2) and (6), the following comprehensive analytical expression of f_T can be obtained [16]

$$f_T = \frac{3}{2}\left[\frac{\mu C_{dep}^2 (kT/q)^3}{2n\pi L^3 C_{ox}^2}\right]\left[1-\exp\left[-\frac{V_{ds}}{kT/q}\right]\right]^2\left[\frac{\exp\left[\frac{2q}{nkT}\left(V_{gs}-V_t\right)\right]}{3\left(V_{gs}-V_t\right)^2-\frac{q}{nkT}\left(V_{gs}-V_t\right)^3}\right] \tag{16}$$

Similar to ΔC_g, Δf_T can be mathematically defined as [16]

$$\Delta f_T \triangleq f_T(\Delta V_t, \Delta W, \Delta L, \ldots) - f_T \tag{17}$$

where f_T stands for the nominal transition frequency in this context.

By also keeping in mind that ΔV_t is the most influential, the following comprehensive analytical expression of Δf_T has been proposed in [16] where the aforesaid physical level differences between N-type and P-type MOSFETs have also been taken into account.

$$\Delta f_{TN} = \frac{\mu C_{dep}^2 (kT/q)^3\left[1-\exp\left[-\frac{V_{ds}}{(kT/q)}\right]\right]^2\left(V_{FB}+2\phi_F+C_{ox}^{-1}\sqrt{2q\varepsilon_{Si}N_a\left(2\phi_F+V_{sb}\right)}-V_t\right)}{\pi n L^3 C_{ox}^2\left(V_{gs}-V_{FB}-2\phi_F-C_{ox}^{-1}\sqrt{2q\varepsilon_{Si}N_a\left(2\phi_F+V_{sb}\right)}\right)^3} \tag{18}$$

$$\Delta f_{TP} = \frac{\mu C_{dep}^2 (kT/q)^3\left[1-\exp\left[-\frac{V_{ds}}{(kT/q)}\right]\right]^2\left(V_{FB}-|2\phi_F|-C_{ox}^{-1}\sqrt{2q\varepsilon_{Si}N_d\left(|2\phi_F|-V_{sb}\right)}-V_t\right)^{-1}}{\pi n L^3 C_{ox}^2\left(V_{gs}-V_{FB}+|2\phi_F|+C_{ox}^{-1}\sqrt{2q\varepsilon_{Si}N_d\left(|2\phi_F|-V_{sb}\right)}\right)^3} \tag{19}$$

It is noted that Δf_{TN} and Δf_{TP} are Δf_T of N-type and P-type MOSFETs, respectively. By also using the up-to-date analytical model of statistical variation in MOSFET's parameter, we have [16]

$$Var\left[\Delta f_{TN}\right] = \frac{\mu^2 C_{dep}^4 (kT)^6 q^{-4} N_{eff} W_{dep} \left[1 - \exp\left[-\frac{Vds}{kT/q}\right]\right]^4 V_t^{-1} \left(V_{FB} + 2\phi_F + C_{ox}^{-1}\sqrt{2q\varepsilon_{Si}N_a\left(2\phi_F + V_{sb}\right)}\right)}{3\pi^2 n^2 W L^7 C_{ox}^6 \left(V_{gs} - V_{FB} - 2\phi_F - C_{ox}^{-1}\sqrt{2q\varepsilon_{Si}N_a\left(2\phi_F + V_{sb}\right)}\right)^6} \tag{20}$$

$$Var\left[\Delta f_{TP}\right] = \frac{\mu^2 C_{dep}^4 (kT)^6 q^{-4} N_{eff} W_{dep} \left[1 - \exp\left[-\frac{Vds}{kT/q}\right]\right]^4 V_t^{-1} \left(V_{FB} - |2\phi_F| - C_{ox}^{-1}\sqrt{2q\varepsilon_{Si}N_d\left(|2\phi_F| - V_{sb}\right)}\right)}{3\pi^2 n^2 W L^7 C_{ox}^6 \left(V_{gs} - V_{FB} + |2\phi_F| + C_{ox}^{-1}\sqrt{2q\varepsilon_{Si}N_d\left(|2\phi_F| - V_{sb}\right)}\right)^6} \tag{21}$$

At this point, it can be stated that the comprehensive analytical model of Δf_T proposed in [16] is composed of Eqs. (18), (19), (20), and (21). For verification, $(Var[\Delta f_{TN}])^{0.5}$ and $(Var[\Delta f_{TP}])^{0.5}$ calculated by using the proposed model have also been compared with their corresponding 65 nm CMOS technology-based benchmarks obtained from the Monte Carlo simulation. The results have been redrawn here in **Figures 4** and **5** where strong agreements to the benchmarks of the model-based $(Var[\Delta f_{TN}])^{0.5}$ and $(Var[\Delta f_{TP}])^{0.5}$ can be observed. The average deviations have been found to be 8.22947 and 6.25104%, respectively [16]. Moreover, it has been proposed in [16] that there exists a very strong statistical relationship between ΔC_g and Δf_T of any certain subthreshold MOSFET as it has been found by using the proposed model that the magnitude of the statistical correlation coefficient of ΔC_g and Δf_T is unity for both N-type and P-type devices.

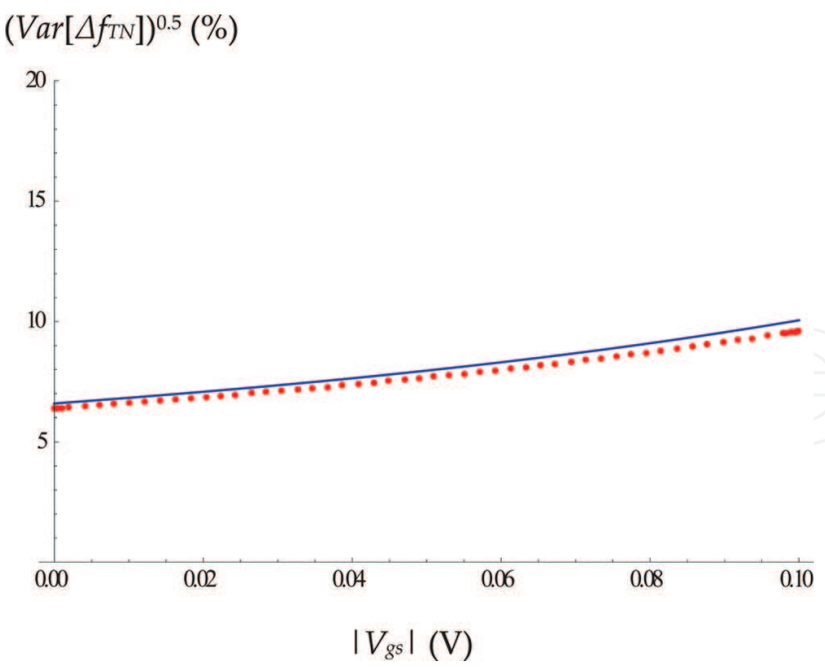

Figure 4. Comparative plot of the model-based $(Var[\Delta f_{TN}])^{0.5}$ (line) and the Monte Carlo simulation-based $(Var[\Delta f_{TN}])^{0.5}$ (dotted) with respect to V_{gs} [16].

http://dx.doi.org/10.5772/intechopen.72710

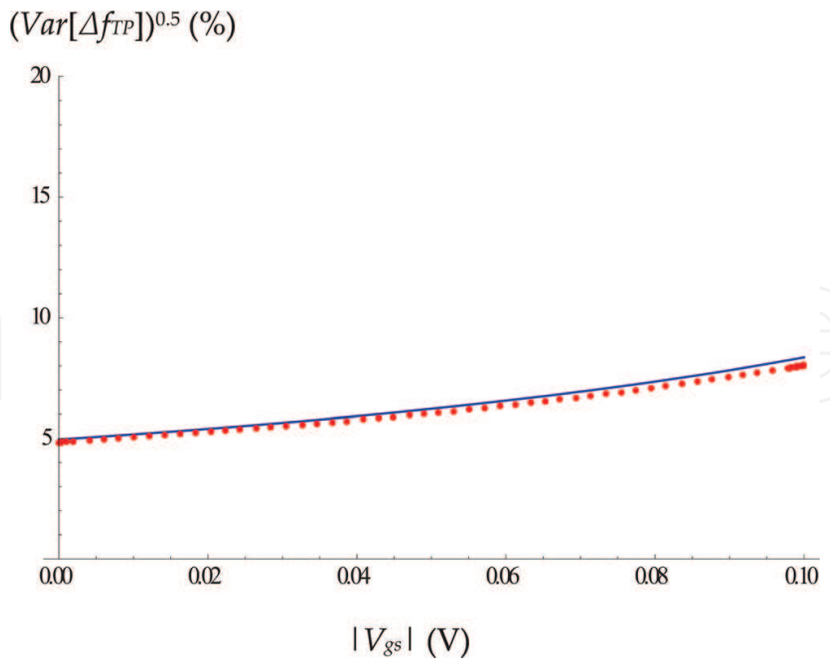

Figure 5. Comparative plot of the model-based $(Var[\Delta f_{TP}])^{0.5}$ (line) and the Monte Carlo simulation-based $(Var[\Delta f_{TP}])^{0.5}$ (dotted) with respect to V_{gs} [16].

5. Variation in maximum frequency of oscillation (f_{max})

Before reviewing the model of variation in f_{max} of subthreshold MOSFET, it is worthy to introduce its definition and mathematical expression. The f_{max}, which takes the effect of the resistance of gate metallization into account, can be defined as the frequency at which the power gain of MOSFET becomes unity. Such gate metallization belonged to the extrinsic part of MOSFET. According to [17], f_{max} can be given under an assumption that C_g is equally divided between drain and source by

$$f_{max} = \frac{1}{4\pi C_g}\sqrt{\frac{2g_m}{R_g}} \tag{22}$$

where R_g stands for the resistance of gate metallization [17].

By substituting g_m and C_g as respectively given by Eqs. (2) and (6) into Eq. (22), we have

$$f_{max} = \frac{\sqrt{\frac{2\mu}{n}\left[\exp\left[-\frac{V_{gs}-V}{nkT/q}\right]\right]^{-1}\left[1-\exp\left[-\frac{V_{ds}}{kT/q}\right]\right]}}{\frac{4\pi}{3}\sqrt{\frac{W}{C_{dep}R_g}}\left[\frac{L^{2.5}C_{ox}^2}{(kT/q)}\right]\left[3\left(V_{gs}-V_t\right)^2-\frac{\left(V_{gs}-V_t\right)^3}{nkT/q}\right]} \tag{23}$$

Similar to the other variations, Δf_{max} can be mathematically defined as [17]

$$\Delta f_{max} \triangleq f_{max}(\Delta V_t, \Delta W, \Delta L, \ldots) - f_{max} \tag{24}$$

where f_{max} stands for the nominal maximum frequency of oscillation in this context.

In [17], the comprehensive analytical model of Δf_{max} have been proposed. Such model is composed of the following equations.

$$\begin{aligned}\Delta f_{max} = & \frac{1}{\sqrt{2}\pi}\left(\frac{\mu}{nR_g}\right)^{\frac{1}{2}}\left[1-\exp\left[-\frac{V_{ds}}{kT/q}\right]\right]^{\frac{1}{2}}\left(\frac{kT}{q}\right)\exp\left[\frac{V_{gs}-V_t}{2nkT/q}\right]\left[\left(\frac{C_{dep}W}{L}\right)^{\frac{1}{2}}\right. \\ & +\left[1-\exp\left[-\tfrac{V_{ds}}{kT/q}\right]\right]^{-1}\left(\tfrac{WL}{C_{dep}}\right)^{\frac{3}{2}}\left(\tfrac{C_{ox}}{kT/q}\right)^{2}\times\left[V_{gs}-V_{FB}-\phi_s-N_{eff}W_{dep}\right] \\ & \left.\times\left[V_t-V_{FB}-\phi_s-N_{eff}W_{dep}\right]\right]\end{aligned} \tag{25}$$

$$\begin{aligned}Var\left[\Delta f_{max}\right] = & \frac{\mu q 4 N_{eff} W_{dep} W^2}{\pi^2 n C_{dep} R_g \varepsilon_0^2 k^2 T^2}\left[\exp\left[-\frac{V_{ds}}{kT/q}\right]-1\right]^{-1}\exp\left[\frac{V_{gs}-V_t}{nkT/q}\right]\left(\frac{kT}{q}\right)^2 \\ & \left[V_{gs}-V_{FB}-\phi_s-N_{eff}W_{dep}\right]^2\end{aligned} \tag{26}$$

It is noted that Eq. (25) has been derived by also keeping in mind that ΔVt is the most dominant. Moreover, Eq. (26) has been formulated based on Eq. (25) and the traditional model of statistical variation in MOSFET's parameter. The model-based $(Var[\Delta f_{max}])^{0.5}$ has been compared with its 65 nm CMOS technology-based benchmarks obtained by the Monte Carlo simulation for verification. The strong agreements between the model-based $(Var[\Delta f_{max}])^{0.5}$ and the benchmark can be observed from the whole simulated range of V_{gs} given by 0–100 mV. The average deviation has been found to be 9.17682 and 8.51743% for N-type and P-type subthreshold MOSFETs, respectively, [17].

Unfortunately, the model proposed in [17] did not take the physical level differences between N-type and P-type MOSFETs into account. By taking such physical level differences into consideration, we have

$$\begin{aligned}\Delta f_{maxN} = & \frac{1}{\sqrt{2}\pi}\left(\frac{\mu}{nR_g}\right)^{\frac{1}{2}}\left[1-\exp\left[-\frac{V_{ds}}{kT/q}\right]\right]^{\frac{1}{2}}\left(\frac{kT}{q}\right)\exp\left[\frac{V_{gs}-V_t}{2nkT/q}\right]\left[\left(\frac{C_{dep}W}{L}\right)^{\frac{1}{2}}\right. \\ & +\left[1-\exp\left[-\tfrac{V_{ds}}{kT/q}\right]\right]^{-1}\left(\tfrac{WL}{C_{dep}}\right)^{\frac{3}{2}}\left(\tfrac{C_{ox}}{kT/q}\right)^{2}\times\left[V_{gs}-V_{FB}-2\phi_F-C_{ox}^{-1}\sqrt{2q\varepsilon_{Si}N_a\left(2\phi_F+V_{sb}\right)}\right] \\ & \left.\times\left[V_t-V_{FB}-2\phi_F-C_{ox}^{-1}\sqrt{2q\varepsilon_{Si}N_a\left(2\phi_F+V_{sb}\right)}\right]\right]\end{aligned} \tag{27}$$

$$\begin{aligned}\Delta f_{maxP} = & \frac{1}{\sqrt{2}\pi}\left(\frac{\mu}{nR_g}\right)^{\frac{1}{2}}\left[1-\exp\left[-\frac{V_{ds}}{kT/q}\right]\right]^{\frac{1}{2}}\left(\frac{kT}{q}\right)\exp\left[\frac{V_{gs}-V_t}{2nkT/q}\right]\left[\left(\frac{C_{dep}W}{L}\right)^{\frac{1}{2}}\right. \\ & +\left[1-\exp\left[-\tfrac{V_{ds}}{kT/q}\right]\right]^{-1}\left(\tfrac{WL}{C_{dep}}\right)^{\frac{3}{2}}\left(\tfrac{C_{ox}}{kT/q}\right)^{2}\times\left[V_{gs}-V_{FB}+\left|2\phi_F\right|+C_{ox}^{-1}\sqrt{2q\varepsilon_{Si}N_d\left(\left|2\phi_F\right|-V_{sb}\right)}\right] \\ & \left.\times\left[V_t-V_{FB}+\left|2\phi_F\right|+C_{ox}^{-1}\sqrt{2q\varepsilon_{Si}N_d\left(\left|2\phi_F\right|-V_{sb}\right)}\right]\right]\end{aligned} \tag{28}$$

where Δf_{maxN} and Δf_{maxP} are Δf_{max} of N-type and P-type MOSFETs, respectively. By using the up-to-date analytical model of statistical variation in MOSFET's parameter, we have

$$Var\left[\Delta f_{maxN}\right] = \frac{3q^2 N_{eff} W_{dep} W^{-3} L^{-1} (\mu / nR_g)(kT/q)^2}{2\pi^2 V_t^{-1}\left[V_{FB} + 2\phi_F + C_{ox}^{-1}\sqrt{2q\varepsilon_{Si} N_a (2\phi_F + V_{sb})}\right]}\left[1 - \exp\left[-\frac{V_{ds}}{kT/q}\right]\right]$$
$$\left[\exp\left[\frac{V_{gs} - V_t}{2nkT/q}\right]\right]^2 \times \left[\left(\frac{C_{dep} W}{L}\right)^{\frac{1}{2}} + \left[1 - \exp\left[-\frac{V_{ds}}{kT/q}\right]\right]^{-1}\left(\frac{WL}{C_{dep}}\right)^{\frac{3}{2}}\left(\frac{C_{ox}}{kT/q}\right)^2\right. \quad (29)$$
$$\left.\times \left[V_{gs} - V_{FB} - 2\phi_F - C_{ox}^{-1}\sqrt{2q\varepsilon_{Si} N_a (2\phi_F + V_{sb})}\right]\right]$$

$$Var\left[\Delta f_{maxP}\right] = \frac{3q^2 N_{eff} W_{dep} W^{-3} L^{-1} (\mu / nR_g)(kT/q)^2}{2\pi^2 V_t^{-1}\left[V_{FB} + 2\phi_F + C_{ox}^{-1}\sqrt{2q\varepsilon_{Si} N_a (2\phi_F + V_{sb})}\right]}\left[1 - \exp\left[-\frac{V_{ds}}{kT/q}\right]\right]$$
$$\left[\exp\left[\frac{V_{gs} - V_t}{2nkT/q}\right]\right]^2 \times \left[\left(\frac{C_{dep} W}{L}\right)^{\frac{1}{2}} + \left[1 - \exp\left[-\frac{V_{ds}}{kT/q}\right]\right]^{-1}\left(\frac{WL}{C_{dep}}\right)^{\frac{3}{2}}\left(\frac{C_{ox}}{kT/q}\right)^2\right. \quad (30)$$
$$\left.\times \left[V_{gs} - V_{FB} + |2\phi_F| + C_{ox}^{-1}\sqrt{2q\varepsilon_{Si} N_d (|2\phi_F| - V_{sb})}\right]\right]$$

At this point, it can be seen that the improved model of Δf_{max} is composed of Eqs. (27), (28), (29), and (30). For verification, the model-based $(Var[\Delta f_{maxN}])^{0.5}$ and $(Var[\Delta f_{maxP}])^{0.5}$ have been compared with their corresponding 65 nm CMOS technology-based benchmarks obtained by

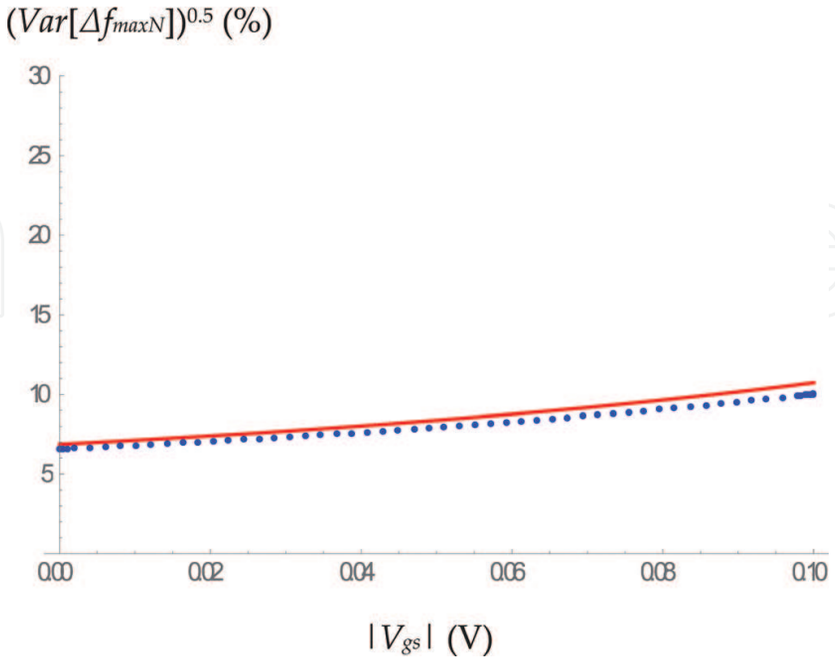

Figure 6. Comparative plot of the model-based $(Var[\Delta f_{maxN}])^{0.5}$ (line) and the Monte Carlo simulation-based $(Var[\Delta f_{maxN}])^{0.5}$ (dotted) with respect to V_{gs}.

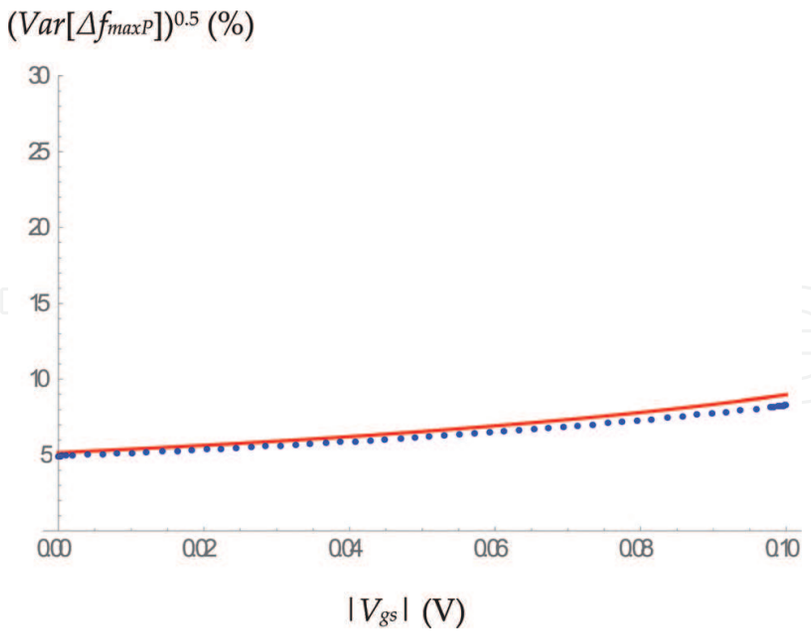

Figure 7. Comparative plot of the model-based $(Var[\Delta f_{maxP}])^{0.5}$ (line) and the Monte Carlo simulation-based $(Var[\Delta f_{maxP}])^{0.5}$ (dotted) with respect to V_{gs}.

using the Monte Carlo simulation. The results are as shown in **Figures 6** and **7** where strong agreements to the benchmarks of the model-based $(Var[\Delta f_{maxN}])^{0.5}$ and $(Var[\Delta f_{maxP}])^{0.5}$ can be observed. The average deviations from the benchmarks have been found to be 6.11788 and 5.85574% for $(Var[\Delta f_{maxN}])^{0.5}$ and $(Var[\Delta f_{maxP}])^{0.5}$, respectively, which are lower than those of the model proposed in [17]. Therefore, our improved model Δf_{max} is also more accurate than the previous one apart from being more detailed as the physical level differences between N-type and P-type MOSFETs have also been taken into account.

Before proceeding further, it should be mentioned here that C_g has more severe variations compared to the other high-frequency characteristics and the P-type subthreshold MOSFET is more robust than the N-type as can be seen from **Figures 2–7**. Moreover, it can be implied that there exists a strong correlation between Δf_{max} and Δf_T as f_{max} is related to f_T by Eq. (31). An implication of strong correlation between Δf_{max} and ΔC_g can be similarly obtained by observing Eq. (22) that is given as

$$f_{max} = \frac{f_T}{\sqrt{2g_m R_g}} \tag{31}$$

6. Some interesting issues

6.1. Statistical/variability aware design trade-offs

For the optimum statistical/variability aware design of any MOSFET-based VHF circuit, ΔC_g, Δf_T, and Δf_{max} must be minimized. It has been found from Eqs. (13), (14), (20), (21), (29), and (30) that $Var[\Delta C_g] \propto L^3$, $Var[\Delta f_T] \propto L^{-7}$ and $Var[\Delta f_{max}] \propto L^{-1}$ for both types of MOSFET. Therefore, it can be seen that shrinking L can reduce ΔC_g of the subthreshold MOSFET of any type

with the increasing Δf_T and Δf_{max} as penalties. Moreover, we have also found that $Var[\Delta C_g] \propto T^{-2}$, $Var[\Delta f_T] \propto T^6$, and $Var[\Delta f_{max}] \propto T^2$. This means that we can reduce Δf_T and Δf_{max} by lowering T with higher ΔC_g as a cost. These design trade-offs must be taken into account in the statistical/variability aware design of any subthreshold MOSFET-based VHF circuits/systems.

6.2. Variation in any high-frequency parameter

Occasionally, determining the variation in other high-frequency parameters apart from C_g, f_T, and f_{max} e.g., bandwidth, f_{BW}, etc., has been found to be necessary. The determination of variation in f_{BW} as a function of Δf_T has been shown in [16]. In general, let any high-frequency parameter of the subthreshold MOSFET be P, the amount of its variation, ΔP, can be determined given the amounts of ΔC_g, Δf_T, and Δf_{max} if P depends on C_g, f_T, and f_{max}. It is noted that the amounts of ΔC_g, Δf_T, and Δf_{max} can be predetermined by using the reviewed comprehensive analytical models. Mathematically, ΔP can be expressed in terms of ΔC_g, Δf_T, and Δf_{max} as follows

$$\Delta P = \left(\frac{\partial P}{\partial C_g}\right)\Delta C_g + \left(\frac{\partial P}{\partial f_T}\right)\Delta f_T + \left(\frac{\partial P}{\partial f_{max}}\right)\Delta f_{max} \tag{32}$$

Therefore, the variance of ΔP, $Var[\Delta P]$ can be given by keeping the aforementioned strong statistical relationships among ΔC_g, Δf_T, and Δf_{max} in mind as follows

$$\begin{aligned} Var[\Delta, P] = \; & \left(\frac{\partial P}{\partial C_g}\right)^2 Var[\Delta_{Cg}] + \left(\frac{\partial P}{\partial f_T}\right)^2 Var[\Delta f_T] + \left(\frac{\partial P}{\partial f_{max}}\right)^2 Var[\Delta f_{max}] \\ & + 2\left(\frac{\partial P}{\partial C_g}\right)\left(\frac{\partial P}{\partial f_T}\right)\sqrt{Var[\Delta_{Cg}]Var[\Delta f_T]} + 2\left(\frac{\partial P}{\partial C_g}\right)\left(\frac{\partial P}{\partial f_{max}}\right)\sqrt{Var[\Delta_{Cg}]Var[\Delta f_{max}]} \\ & + 2\left(\frac{\partial P}{\partial f_T}\right) \times \left(\frac{\partial P}{\partial f_{max}}\right)\sqrt{Var[\Delta f_T]Var[\Delta f_{max}]} \end{aligned} \tag{33}$$

Noted also that the $Var[\Delta C_g]$, $Var[\Delta f_T]$, and $Var[\Delta f_{max}]$ can be known by applying those reviewed models.

6.3. High-frequency parameter mismatches

The amount of mismatches in C_g, f_T, and f_{max} of multiple subthreshold MOSFETs can be determined by applying those reviewed comprehensive analytical models of ΔC_g, Δf_T, and Δf_{max} even though they are dedicated to a single device. As an illustration, the mismatches in C_g, f_T, and f_{max} of two deterministically identical subthreshold MOSFETs, i.e., M1 and M2, will be determined. Traditionally, the magnitude of mismatch can be measured by using its variance [22]. Let the mismatches in C_g, f_T, and f_{max} of M1 and M2 be denoted by ΔC_{g12}, Δf_{T12}, and Δf_{max12}, respectively, their variances, i.e., $Var[\Delta C_{g12}]$, $Var[\Delta f_{T12}]$, and $Var[\Delta f_{max12}]$, can be respectively related to $Var[\Delta C_g]$, $Var[\Delta f_T]$, and $Var[\Delta f_{max}]$ of M1 and M2, which can be determined by using those reviewed models, via the following equations

$$Var\left[\Delta C_{g12}\right] = Var\left[\Delta C_{g1}\right] + Var\left[\Delta C_{g2}\right] - 2\rho_{\Delta C_{g1}\Delta C_{g2}}\sqrt{Var\left[\Delta C_{g1}\right]Var\left[\Delta C_{g2}\right]} \tag{34}$$

$$Var\left[\Delta f_{T12}\right] = Var\left[\Delta f_{T1}\right] + Var\left[\Delta f_{T2}\right] - 2\rho_{\Delta C_{g1}\Delta C_{g2}}\sqrt{Var\left[\Delta f_{T1}\right]Var\left[\Delta f_{T2}\right]} \tag{35}$$

$$Var\left[\Delta f_{max12}\right] = Var\left[\Delta f_{max1}\right] + Var\left[\Delta f_{max2}\right] - 2\rho_{\Delta C_{g1}\Delta C_{g2}}\sqrt{Var\left[\Delta f_{max1}\right]Var\left[\Delta f_{max2}\right]} \tag{36}$$

It is noted that ΔC_{gi}, Δf_{Ti}, Δf_{maxi}, $Var[\Delta C_{gi}]$, $Var[\Delta f_{Ti}]$, and $Var[\Delta f_{maxi}]$, respectively, denote ΔC_g, Δf_T, Δf_{max}, $Var[\Delta C_g]$, $Var[\Delta f_T]$, and $Var[\Delta f_{max}]$ of Mi where $\{i\} = \{1, 2\}$. Moreover, ρ_{XY} stands for the correlation coefficient of X and Y where $\{X\} = \{\Delta C_{g1}, \Delta f_{T1}, \Delta f_{max1}\}$ and $\{Y\} = \{\Delta C_{g2}, \Delta f_{T2}, \Delta f_{max2}\}$. For closely spaced MOSFETs with positive correlation, ρ_{XY}can be given by 1 as the statistical correlation between closely spaced devices is very strong [22]. As a result, the mismatches are maximized. If the negative correlation is assumed on the other hand, ρ_{XY} become -1 and the mismatches are minimized [16]. For distanced devices, we have, $\rho_{XY} = 0$ as the correlation is very weak and can be neglected.

If we assume that both M1 and M2 are statistically identical, we have $Var[\Delta C_{g1}] = Var[\Delta C_{g2}] = Var[\Delta C_g]$, $Var[\Delta f_{T1}] = Var[\Delta f_{T2}] = Var[\Delta f_T]$, and $Var[\Delta f_{max1}] = Var[\Delta f_{max2}] = Var[\Delta f_{max}]$. Thus, Eqs. (34), (35), and (36) become

$$Var\left[\Delta C_{g12}\right] = 2Var\left[\Delta C_g\right]\left(1 - \rho_{\Delta C_{g1}\Delta C_{g2}}\right) \tag{37}$$

$$Var\left[\Delta f_{T12}\right] = 2Var\left[\Delta f_{T1}\right]\left(1 - \rho_{\Delta f_{T1}\Delta f_{T2}}\right) \tag{38}$$

$$Var\left[\Delta f_{max12}\right] = 2Var\left[\Delta f_{max1}\right]\left(1 - \rho_{\Delta f_{max1}\Delta f_{max2}}\right) \tag{39}$$

From these equations, it can be seen that $Var[\Delta C_{g12}]$, $Var[\Delta f_{T12}]$, and $Var[\Delta f_{max12}]$ can all be approximately given by 0 if those statistically identical devices are closely spaced and positively correlated as all ρ_{XY}'s are given by 1. This implies that the high-frequency parameter mismatches of statistically identical, closely spaced, and positively correlated subthreshold MOSFETs can be neglected.

6.4. Variation in any VHF circuit/system

By using the reviewed models, the variation in the crucial parameter of any subthreshold MOSFET-based VHF circuit/system can be analytically formulated. As a case study, the subthreshold MOSFET-based Wu current-reuse active inductor proposed in [1] will be considered. This active inductor can be depicted as shown in **Figure 8**. According to [1], the inductance, l, of this active inductor can be given by

$$l = \frac{C_{g1}}{g_{m1}g_{m2}} \tag{40}$$

http://dx.doi.org/10.5772/intechopen.72710

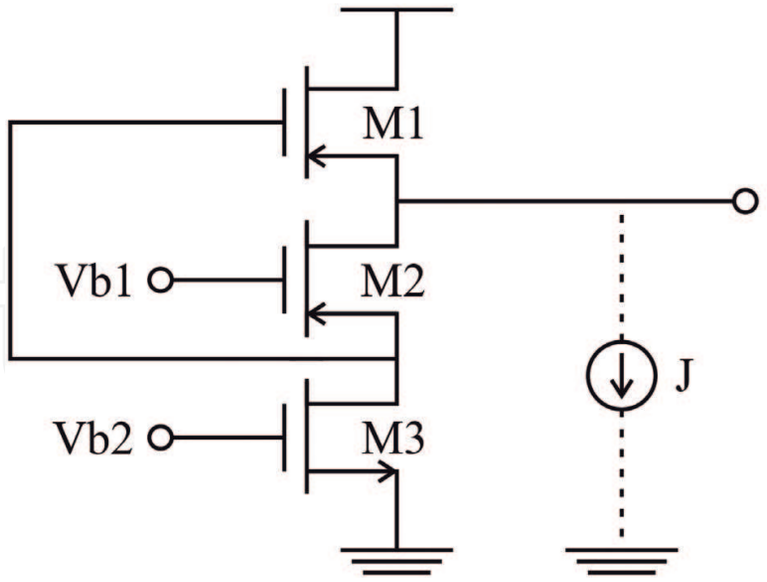

Figure 8. Wu current-reuse active inductor [1].

where C_{g1}, g_{m1}, and g_{m2} are gate capacitance of M1, transconductance of M1, and transconductance of M2, respectively.

By using Eq. (40), the variation in l, Δl due to the variation in C_{g1}, ΔC_{g1} can be immediately given by [16]

$$\Delta l = \frac{\Delta C_{g1}}{g_{m1} g_{m2}} \tag{41}$$

Therefore, we have the following relationship between the variances of Δl and ΔC_{g1}

$$Var[\Delta l] = \frac{Var\left[\Delta C_{g1}\right]}{g_{m1} g_{m2}} \tag{42}$$

It is noted that $Var[\Delta C_{g1}]$ can be determined by using those reviewed models. It can also be seen that $Var[\Delta l] \propto Var\left[\Delta C_{g1}\right]$ and $Var[\Delta l] \propto 1/g_{m1} g_{m2}$ [16]. Therefore, it is far more convenient to minimize Δl by reducing g_{m1} and g_{m2} as they are electronically controllable unlike ΔC_{g1}, which must be minimized at the physical level by lowering L as stated above.

6.5. Reduced computational effort simulation

If we let the key parameter of any subthreshold MOSFET-based VHF circuit/system with M MOSFETs under consideration be Z, its variance, $Var[Z]$, which is the desired statistical/variability aware simulation result, can be given by.

$$
\begin{aligned}
Var[Z] = & \sum_{i=1}^{M}\left[\left(S_{C_{gi}}^{Z}\right)^{2}\sigma_{\Delta C_{gi}}^{2}+\left(S_{f_{Ti}}^{Z}\right)^{2}\sigma_{\Delta f_{Ti}}^{2}+\left(S_{f_{maxi}}^{Z}\right)^{2}\sigma_{\Delta f_{maxi}}^{2}\right] \\
& +\sum_{i\neq j}^{M}\sum_{j=1}^{M}\left[\left(S_{C_{gi}}^{Z}\right)\left(S_{C_{gj}}^{Z}\right)\rho_{\Delta C_{gi}\Delta C_{gj}}\sqrt{\sigma_{\Delta C_{gi}}^{2}}\sqrt{\sigma_{\Delta C_{gj}}^{2}}+\left(S_{f_{Ti}}^{Z}\right)\left(S_{f_{Tj}}^{Z}\right)\rho_{\Delta f_{Ti}\Delta f_{Tj}}\sqrt{\sigma_{\Delta f_{Ti}}^{2}}\sqrt{\sigma_{\Delta f_{Tj}}^{2}}\right. \\
& \left.+\left(S_{f_{maxi}}^{Z}\right)\left(S_{f_{maxj}}^{Z}\right)\rho_{\Delta f_{maxi}\Delta f_{maxj}}\sqrt{\sigma_{\Delta f_{maxi}}^{2}}\sqrt{\sigma_{\Delta f_{maxj}}^{2}}\right] \\
& +2\sum_{i=1}^{M}\sum_{j=1}^{M}\left[\left(S_{C_{gi}}^{Z}\right)\left(S_{f_{Ti}}^{Z}\right)\rho_{\Delta C_{gi}\Delta_{fTj}}\sqrt{\sigma_{\Delta C_{gi}}^{2}}\sqrt{\sigma_{\Delta f_{Tj}}^{2}}+\left(S_{C_{gi}}^{Z}\right)\left(S_{f_{maxj}}^{Z}\right)\rho_{\Delta C_{gi}\Delta f_{maxj}}\right. \\
& \left.\sqrt{\sigma_{\Delta C_{gi}}^{2}}\sqrt{\sigma_{\Delta f_{maxj}}^{2}}+\left(S_{f_{Ti}}^{Z}\right)\left(S_{f_{maxj}}^{Z}\right)\rho_{\Delta f_{Ti}\Delta f_{maxj}}\sqrt{\sigma_{\Delta f_{Ti}}^{2}}\sqrt{\sigma_{\Delta f_{maxj}}^{2}}\right]
\end{aligned}
\tag{43}
$$

It is noted that the magnitude of ρ_{XY}, where $\{X\} = \{\Delta C_{gi}, \Delta f_{Ti}, \Delta f_{maxi}\}$, $\{Y\} = \{\Delta C_{gj}, \Delta f_{Tj}, \Delta f_{maxj}\}$, and the subscripts i and j refers to the arbitrary ith and jth MOSFET, respectively, in this scenario, approaches 1 when $i = j$ as it determines the correlation of the same device. Moreover, $S_{C_{gi}}^{Z}\left(S_{C_{gj}}^{Z}\right)$, $S_{f_{Ti}}^{Z}\left(S_{f_{Tj}}^{Z}\right)$, and $S_{f_{maxi}}^{Z}\left(S_{f_{maxj}}^{Z}\right)$ denote the sensitivity of Z to C_g, f_T, and f_{max} of ith (jth) MOSFET, respectively. By using Eq. (43) and the reviewed comprehensive analytical models for predetermining all $Var[X]$'s and $Var[Y]$'s, $Var[Z]$ can be numerically determined in a reduced computational effort manner as those sensitivities can be obtained by using the sensitivity analysis [23], which required much less computational effort compared to the conventional Monte Carlo simulation. This is because the circuit/system of interest is needed to be solved only once for obtaining the sensitivities and then $Var[Z]$ can be immediately determined unlike the Monte Carlo simulation that requires numerous runs in order to reach the similar outcome [16]. Therefore, much of the computational effort can be significantly reduced.

7. Conclusion

In this chapter, the comprehensive analytical models of ΔC_g, Δf_T, and Δf_{max} of subthreshold MOSFET, which serves as the basis of many VHF circuits/systems, have been reviewed. Interesting issues related to these models i.e., statistical/variability aware design trade-offs of subthreshold MOSFET-based VHF circuit/system; determination of variation in any high-frequency parameter and mismatch in C_g, f_T, and f_{max}; determination of variation in any subthreshold MOSFET-based VHF circuit/system; and the computationally efficient statistical/variability aware simulation with sensitivity analysis have been discussed. Moreover, a modified version of the comprehensive analytical model of Δf_{max} has also been proposed. This revised model has been found to be more accurate and detailed than the previous one.

Author details

Rawid Banchuin

Address all correspondence to: rawid.ban@siam.edu

Graduated School of Information Technology and Faculty of Engineering,
Siam University, Thailand

References

[1] Yushi Z, Yuan F. Subthreshold CMOS active inductor with applications to low-power injection-locked oscillators for passive wireless microsystems. In: Proceedings of the IEEE International Midwest Symposium on Circuits and System (MWSCAS '10); August 1–4, 2010. Seatle: IEEE; 2010. pp. 885-888

[2] Perumana BG, Mukhopadhyay R, Chakraborty S, Lee C-H, Laskar J. A low power fully monolithic subthreshold CMOS receiver with integrated LO generation for 2.4 GHz wireless PAN application. IEEE Journal of Solid-State Circuits. 2008;**43**:2229-2238. DOI: 10.1109/JSSC.2008.2004330

[3] Perumana BG, Chakraborty S, Lee C-H, Laskar J. A fully monolithic 260-μW, 1-GHz subthreshold low noise amplifier. IEEE Microwave and Wireless Components Letters. 2005;**15**:428-430. DOI: 10.1109/LMWC.2005.850563

[4] Lee H, Mohammadi S. A 3 GHz subthreshold CMOS low noise amplifier. In: Proceedings of the IEEE Radio Frequency Integrated Circuits Symposium (RFIC'06); June 10–13, 2006. San Francisco: IEEE; 2006. pp. 494-497

[5] Kim S, Choi J, Lee J, Koo B, Kim C, Eum N, Yu H, Jung H. A subthreshold CMOS front-end design for low-power band-III T-DMB/DAB recievers. ETRI Journal. 2011;**33**:969-972. DOI: 10.4218/etrij.11.0211.0055

[6] Masuda H, Kida T, Ohkawa S. Comprehensive matching characterization of analog CMOS circuits. IEICE Transaction on Fundamentals of Electronics, Communications and Computer Sciences. 2009;**E92-A**:966-975. DOI: 10.1587/transfun.E92.A.966

[7] Banchuin R. Process induced random variation models of nanoscale MOS performance: Efficient tool for the nanoscale regime analog/mixed signal CMOS statistical/variability aware design. In: Proceedings of the International Conference on Information and Electronics Engineering (ICIEE '11); May 28–29, 2011. Bangkok: IACSIT Press; 2011. pp. 6-12

[8] Banchuin R. Complete circuit level random variation models of nanoscale MOS performance. International Journal of Information and Electronic Engineering. 2011;**1**:9-15. DOI: 10.7763/IJIEE.2011.V1.2

[9] Weifeng L, Lingling S. Modeling of current mismatch induced by random dopant fluctuation. Journal of Semiconductors. 2011;**32**:084003-1-084003-5. DOI: 10.1088/1674-4926/32/8/084003

[10] Papatanasiou K. A designer's approach to device mismatch: Theory, modeling, simulation techniques, scripting, applications and examples. Analog Integrated Circuits and Signal Processing. 2006;**48**:95-106. DOI: 10.1007/s10470-066-5367-2

[11] Rao R, Srivastava A, Blaauw D, Sylvester D. Statistical analysis of subthreshold leakage current for VLSI circuits. IEEE Transactions on Very Large Scale Integration (VLSI) Systems. 2004;**12**:131-139. DOI: 10.1109/TVLSI.2003.821549

[12] Forti F, Wright ME. Measurement of MOS current mismatch in the weak inversion region. IEEE Journal of Solid-State Circuits. 1994;**29**:138-142. DOI: 10.1109/4.272119

[13] Kim H-S, Chung C, Lim J, Park K, Oh H, Kang H-K. Characterization and modeling of RF-performance (f_T) fluctuation in MOSFETs. IEEE Electron Device Letters. 2009;**30**:855-857. DOI: 10.1109/LED.2009.2023826

[14] Banchuin R. Novel complete probabilistic models of random variation in high frequency performance of nanoscale MOSFET. Journal of Electrical and Computer Engineering. 2013;**2013**:1-10. DOI: 10.1155/2013/189436

[15] Banchuin R, Chaisricharoen R. Analytical analysis and modelling of variation in gate capacitance of subthreshold MOSFET. In: Proceedings of the Joint International Conference Information and Communication Technology, Electronic and Electrical Engineering (JICTEE '14); March 5–8, 2014. Chiang Rai: IEEE. 2014. pp. 1-4

[16] Banchuin R. Analysis and comprehensive analytical modeling of statistical variations in subthreshold MOSFET's high frequency characteristics. Advances in Electrical and Electronic Engineering. 2014;**12**:47-57. DOI: 10.15598/aeee.v12i1.909

[17] Banchuin R, Chaisricharoen R. Analytical analysis and modelling of variation in maximum frequency of oscillation of subthreshold MOSFET. In: Proceedings of the Joint International Conference Information and Communication Technology, Electronic and Electrical Engineering (JICTEE '14); March 5–8, 2014. Chiang Rai: IEEE; 2014. pp. 1-4

[18] Kwong J, Chandrakasan AP. Advances in ultra-low-voltage design. IEEE Solid State Circuits Magazines. 2008;**13**:20-27. DOI: 10.1109/N-SSC.2008.4785819

[19] Pelgrom MJM, Duinmaijer ACJ, Welbers APG. Matching properties of MOS transistors. IEEE Journal of Solid-State Circuits. 1989;**24**:1433-1439. DOI: 10.1109/JSSC.1989.572629

[20] Takeuchi K, Nishida A, Hiramoto T. Random fluctuations in scaled MOS devices. In: Proceedings of the International Conference on Simulation of Semiconductor Processes and Devices (SISPAD '09); September 9–11, 2009. San Diego: IEEE; 2009. pp. 1-7

[21] Razavi B. Design of Analog CMOS Integrated Circuits. Boston: McGraw-Hill; 2001. p. 684

[22] Cathignol A, Mennillo S, Bordez S, Vendrame L, Ghibaudo G. Spacing impact on MOSFET mismatch. In: Proceedings of the IEEE International Conference on Microelectronic Test Structure (ICMTS '08); March 24–27, 2008. Edinburgh: IEEE; 2009. pp. 90-94

[23] Cijan G, Tuma T, Burmen A. Modeling and simulation of MOS transistor mismatch. In: Proceedings of the Eurosim Congress on Modeling and Simulation (EUROSIM '07); September 9–13, 2007. Ljubljana: SLOSIM; 2007. pp. 1-8